Convergent and conservative schemes for nonclassical solutions based on kinetic relations. I.

Benjamin Boutin[1,2], Christophe Chalons[1,3], Frédéric Lagoutière[1,3], and Philippe G. LeFloch[1]

Abstract

We propose a new numerical approach to compute nonclassical solutions to hyperbolic conservation laws. The class of finite difference schemes presented here is fully conservative and keep nonclassical shock waves as sharp interfaces, contrary to standard finite difference schemes. The main challenge is to achieve, at the discretization level, a consistency property with respect to a prescribed kinetic relation. The latter is required for the selection of physically meaningful nonclassical shocks. Our method is based on a reconstruction technique performed in each computational cell that may contain a nonclassical shock. To validate this approach, we establish several consistency and stability properties, and we perform careful numerical experiments. The convergence of the algorithm toward the physically meaningful solutions selected by a kinetic relation is demonstrated numerically for several test cases, including concave-convex as well as convex-concave flux-functions.

1 Introduction

State of the art

We are interested here in the challenging issue of numerically computing *nonclassical* solutions (containing undercompressive shocks) to nonlinear hyperbolic conservation laws. Nonclassical solutions have the distinctive feature of being dynamically driven by small-scale effects such as diffusion, dispersion, and other high-order phenomena. Their selection requires an additional jump relation, called a kinetic relation, and introduced in the context of phase transition dynamics [28, 29, 30, 31, 1, 2, 11, 20, 13, 14, 26, 27], and investigated by LeFloch and collaborators in the context of general hyperbolic systems of conservation laws (see [21] for a review).

From pioneering work by Hayes and LeFloch [13, 14] it is now recognized that standard finite difference schemes do not converge to nonclassical solutions selected by the prescribed kinetic function. In fact, kinetic functions can be associated not only with continuous models, but with the finite difference schemes themselves. Achieving a good agreement between the continuous and the numerical kinetic functions has been found to be very challenging.

[1] Laboratoire Jacques-Louis Lions & Centre National de la Recherche Scientifique, Université Pierre-et-Marie Curie (Paris 6), 75252 Paris Cedex 05, France. E-mail: Boutin@ann.jussieu.fr, LeFloch@ann.jussieu.fr

[2] DEN/DANS/DM2S/SFME/LETR CEA-Saclay, 91191 Gif-sur-Yvette, France.

[3] Université Paris Diderot (Paris 7), 75251 Paris Cedex 05.
E-mail: Chalons@math.jussieu.fr, Lagoutie@math.jussieu.fr

In the present paper, we will show how to enforce the validity of the kinetic relation at the numerical level, and we design a *fully conservative* scheme which combines the advantages of standard finite differences and Glimm-type (see below) approaches.

Nonclassical shocks and other phase transitions are naturally present in many models of continuum physics, especially in the modeling of real fluids governed by complex equations of state. This is the case, for instance, of models describing the dynamics of liquid-vapor phase transitions in compressible fluids, or of solid-solid phase transformations in materials such as memory alloys. For numerical work in this direction we refer to [15, 16, 8, 24, 25].

Setting for this paper

We restrict here attention to scalar conservation laws

$$\begin{array}{l} \partial_t u + \partial_x f(u) = 0, \qquad u(x,t) \in \mathbb{R}, \;\; (x,t) \in \mathbb{R} \times \mathbb{R}^+, \\ u(x,0) = u_0(x), \end{array} \tag{1}$$

and postpone the discussion of systems of conservation laws to the follow-up paper [4]. The above equation must be supplemented with an entropy inequality of the form

$$\partial_t U(u) + \partial_x F(u) \leq 0. \tag{2}$$

Here, t denotes the time variable, x the (one-dimensional) space variable, $f : \mathbb{R} \to \mathbb{R}$ the flux function, and (U, F) is any strictly convex mathematical entropy pair. That is, $U : \mathbb{R} \to \mathbb{R}$ is strictly convex and $F : \mathbb{R} \to \mathbb{R}$ is given by $F' = U' f'$. Equations (1) and (2) are imposed in the distributional sense.

We rely here on the theory of nonclassical solutions based on kinetic relations, established in [21]. The flux f is assumed to be *nonconvex*, which is the source of mathematical and numerical difficulties. From the mathematical standpoint, a single entropy inequality like (2) does not suffice to select a unique solution. This can be seen already at the level of the Riemann problem, corresponding to (1)-(2) when u_0 has the piecewise constant form

$$u_0(x) = \left\{ \begin{array}{ll} u_l, & x < 0, \\ u_r, & x > 0, \end{array} \right. \tag{3}$$

u_l and u_r being constant states. The Riemann problem admits (up to) a one-parameter family of solutions (see Chapter 2 in [21]). However, these solutions contain discontinuities violating the standard Lax shock inequalities, which are referred to as *nonclassical*. They are essential from the physical standpoint, and should be retained. This non-uniqueness can be fixed however, provided an additional algebraic condition, the so-called *kinetic relation,* is imposed on each nonclassical shock. Consider a shock connecting a left-hand state u_- to a right-hand state u_+ and propagating with the speed σ given by the usual Rankine-Hugoniot relation, that is,

$$u(x,t) = \left\{ \begin{array}{ll} u_-, & x < \sigma t, \\ u_+, & x > \sigma t, \end{array} \right. \qquad \sigma = \sigma(u_-, u_+) = \frac{f(u_+) - f(u_-)}{u_+ - u_-}. \tag{4}$$

The kinetic relation takes the form

$$u_+ = \varphi^\flat(u_-) \;\; \text{for all nonclassical shocks}, \tag{5}$$

where $\varphi^\flat$ is the so-called *kinetic function*. Equivalently, denoting by $\varphi^{-\flat}$ the inverse of the kinetic function it may be preferable to write $u_- = \varphi^{-\flat}(u_+)$. The kinetic relation implies that the right-hand (respectively left-hand) state is no longer free (as in a classical shock wave) but depends explicitly on the left-hand (respectively right-hand) state.

Objectives in this paper

At the numerical level, several strategies exist in the literature in order to take into account the kinetic relation (5). We can distinguish between diffuse interface methods and sharp interface methods.

In the first approach, one assumes that the kinetic relation is derived from an augmented continuous model and, in order to take into account the internal structure of nonclassical discontinuities, one attempts to resolve the effects dues to (small) diffusive and dispersive terms that generate them. It is then possible to construct conservative schemes that mimic at the numerical level the effect of the regularized models. Due to the great sensitivity of nonclassical solutions with respect to small scales and numerical diffusion, it turns out that numerical results are satisfactory for shocks with moderate amplitude, but discrepancies between the exact and the numerical kinetic function arise with shocks with large amplitudes and in long-time computations. For this circle of ideas we refer the reader to [13, 14], and the follow-up papers [22, 7, 8].

In the second approach, small scale features are not explicitly taken into account. Instead, the kinetic relation is included, in a way or another, in the design of the numerical scheme. This is the case of the random choice and front tracking schemes. It should be mentioned here that the Glimm scheme and front tracking schemes do converge to exact solutions even in presence of nonconclassical shocks; see [20, 21, 23] for the theoretical aspects and Chalons and LeFloch [9] for a numerical study of the Glimm scheme. These schemes require the explicit knowledge of the underlying nonclassical Riemann solver, which may be expensive numerically, and this motivated the introduction of the so-called transport-equilibrium scheme by Chalons [5, 6].

In [16], Hou, LeFloch, and Zhong proposed a class of converging schemes for the computation of propagating solid-solid phase boundaries. More recently, Merckle and Rohde [25] developed a ghost-fluid type algorithm for a model of dynamics of phase transition. These schemes provide satisfactory numerical results, as nonclassical discontinuities are sharply and accurately computed. Although the convergence of the methods was demonstrated numerically, their main drawback in practice is similar to the Glimm-type schemes and the property of strict conservation of the conservative variable u fails.

Building on these previous works, our objective in this paper is to design a fully conservative, finite difference scheme for the approximation of nonclassical solutions to the hyperbolic conservation law (1). Our basic strategy relies on the discontinuous reconstruction technique proposed recently in Lagoutière [18, 19] which has been found to be particularly efficient to computing *classical* solutions of (1) with moderate numerical diffusion.

In our approach below, the kinetic function $\varphi^\flat$ is included explicitly in the algorithm, in such a way that nonclassical shocks are computed (essentially) *exactly* while classical shocks suffer moderate numerical diffusion. To validate our strategy we perform various numerical experiments and, in particular, draw the kinetic function associated with our scheme. As the mesh is refined, we observe that the approximate kinetic function converges toward the analytic kinetic function. The scheme also enjoys several fundamental stability properties of consistency with the conservative form of the equation and (like the Glimm scheme) with single nonclassical discontinuities.

2 Nonclassical Riemann solver with kinetics

Assumption on the flux-function

We describe here the nonclassical Riemann solver introduced and investigated in LeFloch [21]. Note in passing that this solver was later extended in [23] to include also a nucleation criterion.

Consider the problem (1)-(2)-(5) for a given Riemann initial data (3). Throughout this paper we assume that the flux f is either *concave-convex* or *convex-concave*, that is, satisfies the conditions (for all $u \neq 0$)

$$uf''(u) > 0, \qquad f'''(0) \neq 0, \qquad \lim_{|u|\to+\infty} f'(u) = +\infty, \tag{6}$$

or

$$uf''(u) < 0, \qquad f'''(0) \neq 0, \qquad \lim_{|u|\to+\infty} f'(u) = -\infty, \tag{7}$$

respectively. The functions $f(u) = u^3 + u$ and $f(u) = -u^3 - u$ are prototypes of particular interest, used later in this paper for the validation of the proposed numerical strategy.

Let $\varphi^\natural : \mathbb{R} \to \mathbb{R}$ be the unique function defined by $\varphi^\natural(0) = 0$ and for all $u \neq 0$, $\varphi^\natural(u) \neq u$ is such that the line passing through the points $(u, f(u))$ and $(\varphi^\natural(u), f(\varphi^\natural(u)))$ is tangent to the graph of f at point $(\varphi^\natural(u), f(\varphi^\natural(u)))$:

$$f'(\varphi^\natural(u)) = \frac{f(u) - f(\varphi^\natural(u))}{u - \varphi^\natural(u)}.$$

This function is smooth, monotone decreasing and onto thanks to (6) or (7). We denote by $\varphi^{-\natural} : \mathbb{R} \to \mathbb{R}$ its inverse function.

Concave-convex flux functions

Let us assume that f obeys (6) and let $\varphi^\flat : \mathbb{R} \to \mathbb{R}$ be a kinetic function, that is (by definition) a monotone decreasing and Lipschitz continuous mapping such that

$$\begin{array}{ll} \varphi_0^\flat(u) < \varphi^\flat(u) \leq \varphi^\natural(u), & u > 0, \\ \varphi^\natural(u) \leq \varphi^\flat(u) < \varphi_0^\flat(u), & u < 0. \end{array} \tag{8}$$

From $\varphi^\flat$, we define the function $\varphi^\sharp : \mathbb{R} \to \mathbb{R}$ such that the line passing through the points $(u, f(u))$ and $(\varphi^\flat(u), f(\varphi^\flat(u)))$ with $u \neq 0$ also cuts the graph of the flux function f at point $(\varphi^\sharp(u), f(\varphi^\sharp(u)))$ with $\varphi^\sharp(u) \neq u$ and $\varphi^\sharp(u) \neq \varphi^\flat(u)$:

$$\frac{f(u) - f(\varphi^\flat(u))}{u - \varphi^\flat(u)} = \frac{f(u) - f(\varphi^\sharp(u))}{u - \varphi^\sharp(u)}.$$

The nonclassical Riemann solver associated with (1)-(2)-(3)-(5) is given as follows.
When $u_l > 0$:

(1) If $u_r \geq u_l$, the solution is a rarefaction wave connecting u_l to u_r.

(2) If $u_r \in [\varphi^\sharp(u_l), u_l)$, the solution is a classical shock wave connecting u_l to u_r.

(3) If $u_r \in (\varphi^\flat(u_l), \varphi^\sharp(u_l))$, the solution contains a nonclassical shock connecting u_l to $\varphi^\flat(u_l)$, followed by a classical shock connecting $\varphi^\flat(u_l)$ to u_r.

(4) If $u_r \leq \varphi^\flat(u_l)$, the solution contains a nonclassical shock connecting u_l to $\varphi^\flat(u_l)$, followed by a rarefaction connecting $\varphi^\flat(u_l)$ to u_r.
When $u_l \leq 0$:

(1) If $u_r \le u_l$, the solution is a rarefaction wave connecting u_l to u_r.

(2) If $u_r \in [u_l, \varphi^\sharp(u_l))$, the solution is a classical shock wave connecting u_l to u_r.

(3) If $u_r \in (\varphi^\sharp(u_l), \varphi^\flat(u_l))$, the solution contains a nonclassical shock connecting u_l to $\varphi^\flat(u_l)$, followed by a classical shock connecting $\varphi^\flat(u_l)$ to u_r.

(4) If $u_r \ge \varphi^\flat(u_l)$, the solution contains a nonclassical shock connecting u_l to $\varphi^\flat(u_l)$, followed by a rarefaction connecting $\varphi^\flat(u_l)$ to u_r.

Convex-concave flux functions

We next assume that f satisfies the condition (7). Let $\varphi^\flat : \mathbb{R} \to \mathbb{R}$ be a kinetic function, that is, a monotone decreasing and Lipschitz continuous map such that

$$\begin{array}{ll} \varphi_0^\flat(u) < \varphi^\flat(u) \le \varphi^{-\natural}(u), & u < 0, \\ \varphi^{-\natural}(u) \le \varphi^\flat(u) < \varphi_0^\flat(u), & u > 0. \end{array} \tag{9}$$

We then define $\rho(u,v) \in \mathbb{R}$ if $v \neq u$ and $v \neq \varphi^\natural(u)$ by

$$\frac{f(\rho(u,v)) - f(u)}{\rho(u,v) - u} = \frac{f(v) - f(u)}{v - u}$$

with $\rho(u,v) \neq u$ and $\rho(u,v) \neq v$, and extend the function ρ by continuity otherwise. Note that $\varphi^\sharp(u) = \rho(u, \varphi^\flat(u))$ where $\varphi^\sharp$ is defined as in the case of a concave-convex flux function. The nonclassical Riemann solver associated with (1)-(2)-(3)-(5) is given as follows.

When $u_l > 0$:

(1) If $u_r \ge u_l$, the solution is a classical shock connecting u_l to u_r.

(2) If $u_r \in [0, u_l)$, the solution is a rarefaction wave connecting u_l to u_r.

(3) If $u_r \in (\varphi^\flat(u_l), 0)$, the solution contains a rarefaction wave connecting u_l to $\varphi^{-\flat}(u_r)$, followed by a nonclassical shock connecting $\varphi^{-\flat}(u_r)$ to u_r.

(4) If $u_r \le \varphi^\flat(u_l)$, the solution contains:

(i) a classical shock connecting u_l to $\varphi^{-\flat}(u_r)$, followed by a nonclassical shock connecting $\varphi^{-\flat}(u_r)$ to u_r, if $u_l > \rho(\varphi^{-\flat}(u_r), u_r)$.

(ii) a classical shock connecting u_l to u_r, if $u_l \le \rho(\varphi^{-\flat}(u_r), u_r)$.

When $u_l \le 0$:

(1) If $u_r \le u_l$, the solution is a classical shock connecting u_l to u_r.

(2) If $u_r \in (u_l, 0]$, the solution is a rarefaction wave connecting u_l to u_r.

(3) If $u_r \in (0, \varphi^\flat(u_l))$, the solution contains a rarefaction wave connecting u_l to $\varphi^{-\flat}(u_r)$, followed by a non classical shock connecting $\varphi^{-\flat}(u_r)$ to u_r.

(4) If $u_r \ge \varphi^\flat(u_l)$, the solution contains:

(i) a classical shock connecting u_l to $\varphi^{-\flat}(u_r)$, followed by a nonclassical shock connecting $\varphi^{-\flat}(u_r)$ to u_r, if $u_l < \rho(\varphi^{-\flat}(u_r), u_r)$.

(ii) a classical shock connecting u_l to u_r, if $u_l \ge \rho(\varphi^{-\flat}(u_r), u_r)$.

Observe that the convex-concave case can in principle be deduced from the concave-convex case, by replacing f by $-f$ and x by $-x$. Nevertheless, it is useful to keep the above two descriptions in mind, since there is a dramatic difference between the Riemann solvers: the nonclassical shock always connects u_l to $\varphi^\flat(u_l)$ in the concave-convex case, and $\varphi^{-\flat}(u_r)$ to u_r in the convex-concave case. The numerical method we are going to describe must take this feature into account, and as we will explain it is necessary to take into account both $\varphi^\flat$ and $\varphi^{-\flat}$ in the design of the scheme.

3 Motivations and difficulties

Notation

Our aim is to design a scheme for the numerical approximation of the nonclassical solutions to (1)-(2)-(5). To this end, we consider the general class of finite volume methods. Introducing constant space and time lengths Δx and Δt for the space and time discretization, we can set $x_{j+1/2} = j\Delta x$, $j \in \mathbb{Z}$, and $t^n = n\Delta t$, $n \in \mathbb{N}$. The discretization consists, at each time t^n, of a piecewise constant function $x \mapsto u_\nu(x, t^n)$ which should be an approximation of the exact solution $u(x, t^n)$ on the cell $\mathcal{C}_j = [x_{j-1/2}; x_{j+1/2})$:

$$u_\nu(x, t^n) = u_j^n, \qquad x \in C_j, \;\; j \in \mathbb{Z}, \;\; n \in \mathbb{N}.$$

Here, ν refers to the ratio $\Delta t/\Delta x$. The initial data at the time $t = 0$ is denoted by u_0 and we define the sequence $(u_j^0)_{j\in\mathbb{Z}}$:

$$u_j^0 = \frac{1}{\Delta x}\int_{x_{j-1/2}}^{x_{j+1/2}} u_0(x)dx, \qquad j \in \mathbb{Z}. \tag{10}$$

The starting point in the conception of our algorithm is a few conventional interpretation of the constant values u_j^n, $j \in \mathbb{Z}$. As suggested by the proposed initialization (10), u_j^n is usually, and rightly, seen as an approximate value of the average on cell $\mathcal{C}_j$ of the exact solution at time t^n. Integrating equation (1) over the slab $\mathcal{C}_j \times [t^n, t^{n+1}]$ and using Green's formula, it is thus natural to define $(u_j^{n+1})_j$ from $(u_j^n)_j$ and a conservative scheme of the following form

$$u_j^{n+1} = u_j^n - \frac{\Delta t}{\Delta x}(f_{j+1/2}^n - f_{j-1/2}^n), \quad j \in \mathbb{Z}, \tag{11}$$

where $f_{j+1/2}^n$ represents an approximate value of the flux that passes through the interface $x_{j+1/2}$ between the times t^n and t^{n+1}.
Here, we shall also consider u_j^n as a given information, on cell $\mathcal{C}_j$ and at time t^n, on the structure of the exact Riemann solution associated with inital states $u_l = u_{j-1}^n$ and $u_r = u_{j+1}^n$ which will develop at the next times $t > t^n$. At this stage, one easily realize that if this information is precise (*i.e.* close to what will really happen), then we should be be in a good position to define accurately the numerical fluxes $f_{j+1/2}^n$ and then predict the approximate values of the solution at time t^{n+1}.

Linear advection equation

As a first illustration, let us consider the linear advection with constant velocity $a > 0$, that is, the scalar conservation law with flux $f(u) = au$. In this case, the weak solution to the initial-value problem for (1) is unique, and is given explicitly as $u(t, x) = u_0(x - at)$. Hence, neither the entropy condition (2) nor the kinetic condition (5) are necessary. The basic scheme for approximating this solution is the so-called upwind scheme and corresponds to the choice $f_{j+1/2}^n = au_j^n$ for all $j \in \mathbb{Z}$. Recall that the CFL condition $a\Delta t/\Delta x \leq \alpha$ for a given $\alpha \leq 1$ is mandatory for the stability of the procedure. Figure 1 (left-hand) shows the corresponding numerical solution at time $t = 0.25$ for $a = 1$, $\alpha = 0.5$ and $u_l = 1$, $u_r = 0$ in (3). The mesh contains 100 points per unit. We observe that the numerical solution presents a good agreement with the exact one but contains numerical diffusion. We propose the following interpretation. In some sense, the value u_j^n that we consider as an information on the Riemann solution associated

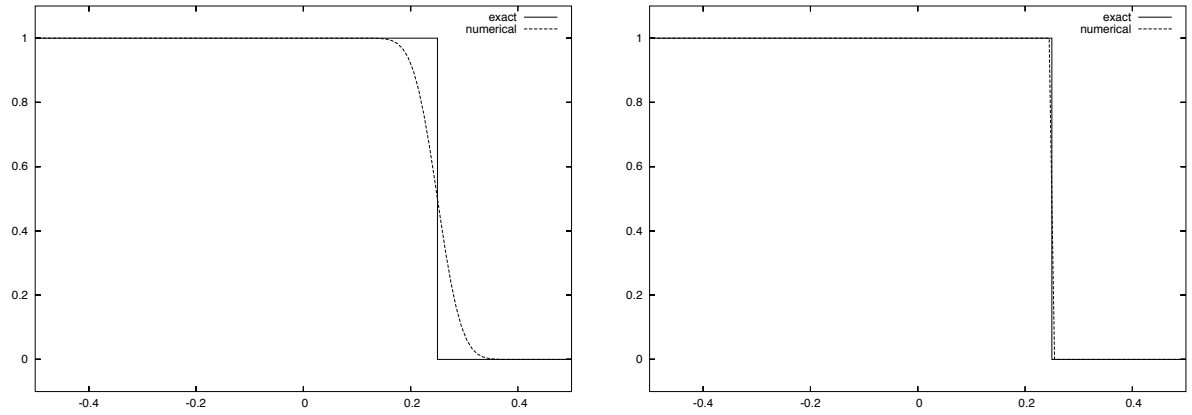

Figure 1: Linear advection - upwind scheme (left-hand) and reconstruction scheme (right-hand).

with initial states $u_l = u^n_{j-1}$ and $u_r = u^n_{j+1}$ is sufficient to correctly approach this solution when defining $f^n_{j+1/2} = au^n_j$, but not enough to avoid the numerical diffusion. Note that the latter is expected but not hoped. In the present situation, the fact is that we actually know what will happen in the future, namely a propagation of the Riemann initial states ($u_l = u^n_{j-1}$ and $u_r = u^n_{j+1}$) with speed a. In particular, no value different from u^n_{j-1} and u^n_{j+1} is created so that information given by u^n_j is clearly not optimal. In the process of calculation of the numerical flux $f^n_{j+1/2}$, we are thus tempted to add more information in the cell $\mathcal{C}_j$ when replacing, as soon as possible, the constant state u^n_j with a discontinuity separating u^n_{j-1} on the left and u^n_{j+1} on the right, and located at point $\overline{x}_j \in \mathcal{C}_j$. In the forthcoming developments, the left and right states of this reconstructed discontinuity will be noted $u^n_{j,l}$ and $u^n_{j,r}$, respectively. Hence, we have here

$$u^n_{j,l} = u^n_{j-1}, \qquad u^n_{j,r} = u^n_{j+1}. \tag{12}$$

See Figure 2 below. We claim that this provides better information for calculating $f^n_{j+1/2}$ than the original one. Such a reconstruction is due to conserve u in order to be relevant, which defines $\overline{x}_j$ by the following constraint

$$(\overline{x}_j - x_{j-1/2})u^n_{j,l} + (x_{j+1/2} - \overline{x}_j)u^n_{j,r} = (x_{j+1/2} - x_{j-1/2})u^n_j$$

which equivalently recast as

$$\overline{x}_j = x_{j-1/2} + \frac{u^n_{j,r} - u^n_j}{u^n_{j,r} - u^n_{j,l}}\Delta x. \tag{13}$$

Then, the reconstruction is possible provided we have $0 \leq d^n_j \leq 1$, with

$$d^n_j = \frac{u^n_{j,r} - u^n_j}{u^n_{j,r} - u^n_{j,l}}. \tag{14}$$

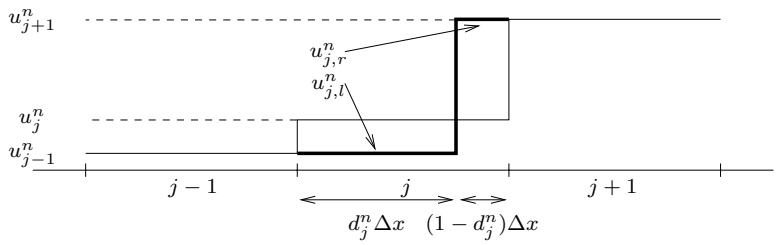

Figure 2: An example of discontinuous reconstruction with conservation property (the linear case).

Now, let us introduce $\Delta t_{j+1/2}$ the time needed by the reconstructed discontinuity to reach the interface $x_{j+1/2}$ (recall that $a > 0$). We clearly have

$$\Delta t_{j+1/2} = \frac{1-d^n_j}{a}\Delta x.$$

In this case, the flux that passes through $x_{j+1/2}$ between times t^n and $t^{n+1} = t^n + \Delta t$ equals $f(u^n_{j,r})$ until $t^n + \Delta t_{j+1/2}$, and $f(u^n_{j,l})$ after (if $\Delta t_{j+1/2} < \Delta t$). Therefore, we propose to set now

$$\Delta t f^n_{j+1/2} = \min(\Delta t_{j+1/2}, \Delta t) f(u^n_{j,r}) + \max(\Delta t - \Delta t_{j+1/2}, 0) f(u^n_{j,l}).$$

On Figure 1 (right-hand), we have plotted the numerical solution given by this new numerical flux, leading to the so-called reconstruction scheme. The parameters of the simulation are the same than those of Figure 1 (left-hand). We see that the more precise informations we have brought on each cell $\mathcal{C}_j$ for calculating the numerical fluxes make the scheme less diffusive than the original one. This strategy was proposed (and is discussed in further details) in [18, 19] (see also [10, 17]). In particular, it is shown therein that the numerical solution presented in Figure 1 (right-hand) is *exact* in the sense that u^n_j equals the average of the exact solution on $\mathcal{C}_j$, that is

$$u^n_j = \frac{1}{\Delta x}\int_{x_{j-1/2}}^{x_{j+1/2}} u(x,t^n)dx, \qquad j \in \mathbb{Z},\ n \in \mathbb{N}. \tag{15}$$

The corresponding numerical discontinuity separating u_l and u_r in then diffused on one cell at most.

Godunov scheme with a nonclassical Riemann solver

As a second illustration, let us go back to the problem (1)-(2)-(5) with a general concave-convex (or convex-concave) flux function f with however, for the sake of clarity,

$$f'(u) \geq 0, \qquad u \in \mathbb{R}. \tag{16}$$

Here, we focus ourselves on a particular Riemann initial data (3) such that $u_r = \varphi^\flat(u_l)$. In other words, the kinetic criterion is imposed on the initial discontinuity. The exact solution then corresponds to the propagation of this discontinuity with speed $\sigma(u_l, u_r) > 0$ given by Rankine-Hugoniot relation:

$$\sigma(u_l, u_r) = \frac{f(u_r) - f(u_l)}{u_r - u_l}. \tag{17}$$

Figure 3 (left-hand) represents the numerical solution given by the upwind scheme $f^n_{j+1/2} = f(u^n_j)$ at time $t = 0.1$, for $f(u) = u^3 + u$ and $u_l = 1$. The kinetic function is taken to be $\varphi^\flat(u) = -0.75\,u$ so that $u_r = -0.75$.

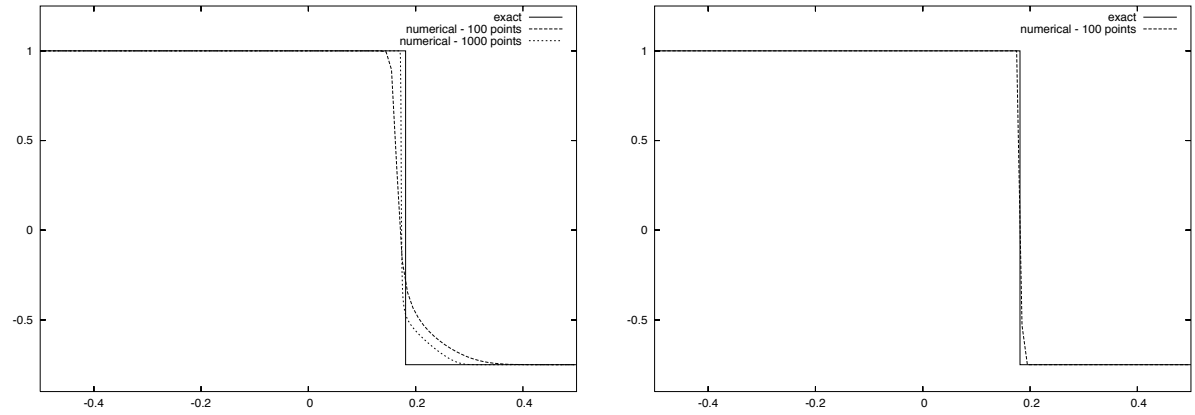

Figure 3: Propagating nonclassical shock - upwind scheme (left-hand) and reconstruction scheme (right-hand).

We observe a strong disagreement between the numerical solution and the exact one. Indeed, the former is made of a (classical) shock followed by a rarefaction wave while the latter is a single (nonclassical) shock from u_l to u_r. It is then clear that the usual upwind scheme (as many others actually) is not adapted for the computation of nonclassical solutions. The next result states that the upwind scheme always converges towards the classical solution of (1)-(2). This scheme is then adapted for the computation of classical solutions only.

Property. *Assume that $u_0 \in L^\infty(\mathbb{R})$ and f is a smooth function satisfying (16). Then, under the CFL condition*

$$\frac{\Delta t}{\Delta x} \max_{u \in A} |f'(u)| \leq 1,$$

with $A := [\min_x u_0(x), \max_x u_0(x)]$ the upwind conservative scheme (11) with $f^n_{j+1/2} = f(u^n_j)$ converges towards the unique classical solution of (1)-(2).

To establish this property, we only need to observe that, under the assumption (16) (propagation is only in one direction), the upwind scheme is equivalent to the standard Godunov scheme associated with the *classical* Riemann solver of (1)-(2) Then, standard compactness and consistency arguments apply and allow us to conclude that the scheme converges towards the unique classical solution.

Obviously, the above property also holds if f is assumed to be decreasing if we define $f^n_{j+1/2} = f(u^n_{j+1})$.

4 A conservative scheme for nonclassical entropy solutions

Preliminaries

In view of the discussion in the previous section and in order to better evaluate the numerical fluxes $f^n_{j+1/2}$, let us obtain some information beyond u^n_j on cell $\mathcal{C}_j$. In the present instance of an isolated propagating discontinuity, it is expected that the Riemann solution associated with initial states u^n_{j-1} and u^n_{j+1} simply propagates the initial discontinuity. This is actually true if

$u_{j-1}^n = u_l$ and $u_{j+1}^n = \varphi^\flat(u_l)$, or more generally if $u_{j+1}^n = \varphi^\flat(u_{j-1}^n)$. So that here again, we propose to replace the constant state u_j^n with a discontinuity separating $u_{j,l}^n$ and $u_{j,r}^n$ and located at point $\overline{x}_j$ given by (13), as soon as possible *i.e.* when $0 \leq d_j^n \leq 1$. We take

$$u_{j,l}^n = \varphi^{-\flat}(u_{j+1}^n) \quad \text{and} \quad u_{j,r}^n = \varphi^\flat(u_{j-1}^n). \tag{18}$$

Note that this reconstruction is equivalent to (12) provided that $u_{j-1}^n = u_l$ and $u_{j+1}^n = \varphi^\flat(u_l)$, or more generally $u_{j+1}^n = \varphi^\flat(u_{j-1}^n)$. Then, under the assumption (16), we again naturally set

$$\Delta t f_{j+1/2}^n = \min(\Delta t_{j+1/2}, \Delta t) f(u_{j,r}^n) + \max(\Delta t - \Delta t_{j+1/2}, 0) f(u_{j,l}^n)$$

with now

$$\Delta t_{j+1/2} = \frac{1 - d_j^n}{\sigma(u_{j,l}^n, u_{j,r}^n)} \Delta x. \tag{19}$$

Figure 3 (right-hand) highlights the benefit of such a reconstruction. The numerical solution now fully agrees with the exact one and is moreover free of numerical diffusion (the profile is composed of a single point). We will show below that it is exact in this case, in the sense that (15) is still valid as in the linear case.

The scheme

On the basis of the above motivations and illustrations, we follow the description of our algorithm by considering the general situation. Assuming as given a sequence $(u_j^n)_{j\in\mathbb{Z}}$ at time t^n, it is thus a question of defining its evolution towards the next time level t^{n+1}. More precisely, and in the context of a finite volume conservative scheme, we have to define the numerical fluxes $(f_{j+1/2}^n)_{j\in\mathbb{Z}}$ coming in (11). For that, we still assume

$$\text{either } f'(u) \geq 0 \text{ for all } u, \quad \text{or } f'(u) \leq 0 \text{ for all } u, \tag{20}$$

so that propagation is in one direction only. According to the previous section, information in cell $\mathcal{C}_j$ is understood as an element of the inner structure of the Riemann problem associated with initial states u_{j-1}^n and u_{j+1}^n. This one will be used to compute either $f_{j+1/2}^n$ (if $f'(u) \geq 0$) or $f_{j-1/2}^n$ (if $f'(u) \leq 0$).
In Section 2, it is stated that the Riemann problem associated with initial states u_{j-1}^n and u_{j+1}^n may contain a nonclassical shock between u_{j-1}^n and $\varphi^\flat(u_{j-1}^n)$ if the function is concave-convex (and between $\varphi^{-\flat}(u_{j+1}^n)$ and u_{j+1}^n if the function is convex-concave).

Recall that these nonclassical waves are difficult to capture numerically and require special attention. (We have shown in the previous section that as many others, the upwind scheme does not suit.) Instead of considering u_j^n as a sufficiently accurate information for the structure of the Riemann solution associated with the initial states u_{j-1}^n and u_{j+1}^n, we propose to replace it (whenever possible) with a discontinuity separating $u_{j,l}^n = \varphi^{-\flat}(u_{j+1}^n)$ on the left and $u_{j,r}^n = \varphi^\flat(u_{j-1}^n)$ on the right, and located at point $\overline{x}_j \in \mathcal{C}_j$. In other words, we propose to introduce in the cell $\mathcal{C}_j$ the right (respectively left) state $\varphi^\flat(u_{j-1}^n)$ (respectively $\varphi^{-\flat}(u_{j+1}^n)$) of the nonclassical discontinuity which is expected to be present in the Riemann solution associated with u_{j-1}^n and u_{j+1}^n (depending on if f obeys (6) or (7)). As in the previous section, one requires the reconstructed discontinuity to satisfy the conservation property (13) and to be located inside $\mathcal{C}_j$, that is $0 \leq d_j^n \leq 1$ with d_j^n given in (14). See Figure 4 for an illustration. Here, we let $u_{j,l}^n = u_{j,r}^n = u_j^n$ if d_j^n given in (14) does not belong to $[0, 1]$.

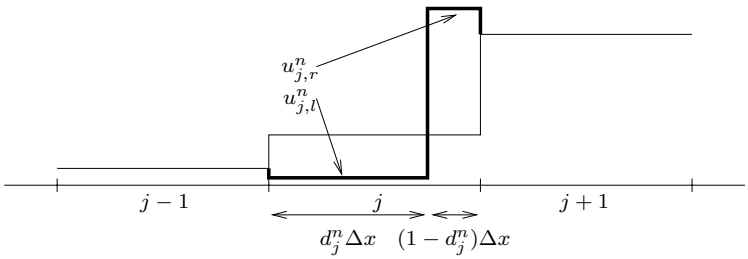

Figure 4: A general discontinuous reconstruction with conservation property (the general case).

Then, we naturally set for all $j \in \mathbb{Z}$:
(i) if f is non-decreasing

$$\Delta t f^n_{j+1/2} = \begin{cases} \min(\Delta t_{j+1/2}, \Delta t) f(u^n_{j,r}) + \max(\Delta t - \Delta t_{j+1/2}, 0) f(u^n_{j,l}), & 0 \le d^n_j \le 1, \\ \Delta t f(u^n_j), & \text{otherwise}, \end{cases} \tag{21}$$

with

$$\Delta t_{j+1/2} = \frac{1 - d^n_j}{\sigma(u^n_{j,l}, u^n_{j,r})} \Delta x. \tag{22}$$

(ii) if f is non-increasing:

$$\Delta t f^n_{j-1/2} = \begin{cases} \min(\Delta t_{j-1/2}, \Delta t) f(u^n_{j,l}) + \max(\Delta t - \Delta t_{j-1/2}, 0) f(u^n_{j,r}), & 0 \le d^n_j \le 1, \\ \Delta t f(u^n_j), & \text{otherwise}, \end{cases} \tag{23}$$

with

$$\Delta t_{j-1/2} = \frac{d^n_j}{-\sigma(u^n_{j,l}, u^n_{j,r})} \Delta x. \tag{24}$$

Note that contrary to the linear advection (see the first illustration in the previous section), the local time step $\Delta t_{j+1/2}$ (respectively $\Delta t_{j-1/2}$) given by (22) (respectively (24)) is now only a prediction of the time needed by the reconstructed discontinuity to reach the interface $x_{j+1/2}$ (respectively $x_{j-1/2}$). The prediction step is however exact in the case of an isolated nonclassical discontinuity (see the second illustration in the previous section) and more generally as soon as u^n_{j-1} and u^n_{j+1} verify $u^n_{j+1} = \varphi^\flat(u^n_{j-1})$.

Observe that the proposed scheme belongs to the class of five-point schemes, since u^{n+1}_j depends on u^n_{j-2}, u^n_{j-1}, u^n_j, u^n_{j+1} and u^n_{j+2}.

Stability and consistency properties

We now state and prove important properties enjoyed by our algorithm.

We assume that the flux f satisfies the monotonicity condition (20) and either the concave-convex or concave-convex conditions (6) or (7) respectively. Then, under the CFL restriction

$$\frac{\Delta t}{\Delta x} \max_u |f'(u)| \le 1, \tag{25}$$

where the maximum is taken over all the u under consideration, the conservative scheme (11) with $f^n_{j+1/2}$ defined for all $j \in \mathbb{Z}$ by (21)-(23) is consistent with (1)-(2)-(5) in the following sense.

Property 1 (Flux consistency.) *Assume that* $u := u_{j-1}^n = u_j^n = u_{j+1}^n$*, then* $f_{j+1/2}^n = f(u)$ *if* $f' \geq 0$ *and* $f_{j-1/2}^n = f(u)$ *if* $f' \leq 0$*.*

Property 2 (Classical solutions.) *Assume that* u_{j-2}^n*,* u_{j-1}^n*,* u_j^n*,* u_{j+1}^n *and* u_{j+2}^n *belong to the same region of convexity of* f*. Then the definition* u_j^{n+1} *given by the conservative scheme (11)-(21)-(23) coincides with the one given by the usual upwind conservative scheme. Then it obeys all the usual stability properties provided by this scheme. In particular, the strategy is convergent if the whole discrete solution belongs to the same region of convexity of* f*.*

Property 3 (Isolated nonclassical shock waves.) *Let* u_l *and* u_r *be two initial states such that* $u_r = \varphi^\flat(u_l)$*. Assume that* $u_j^0 = u_l$ *if* $j \leq 0$ *and* $u_j^0 = u_r$ *if* $j \geq 1$*. Then the conservative scheme (11)-(21)-(23) provides an exact numerical solution on each cell* $\mathcal{C}_j$ *in the sense that*

$$u_j^n = \frac{1}{\Delta x} \int_{x_{j-1/2}}^{x_{j+1/2}} u(x, t^n) dx, \qquad j \in \mathbb{Z}, \ n \in \mathbb{N}, \tag{26}$$

where u *denotes the exact Riemann solution of (1)-(2)-(3)-(5) given by* $u(x,t) = u_l$ *if* $x < \sigma(u_l, u_r)t$ *and* $u(x,t) = u_r$ *otherwise, and is convergent towards* u*. In particular, the numerical discontinuity is diffused on one cell at most.*

The following comments are in order. Property (i) shows that the proposed numerical flux function is consistent in the classical sense of finite volume methods. Properties (ii) and (iii) provide us with crucial stability/accuracy properties. They show that the method is actually convergent if the solution remains in the same region of convexity of f (see (ii)) or, more importantly, the solution consists in an isolated nonclassical discontinuity satisfying the prescribed kinetic relation (see (iii)). We emphasize that all of the *conservative* schemes proposed so far in the literature violate the latter property.

Proof of Property 1. (i) If $u := u_{j-1}^n = u_j^n = u_{j+1}^n$ then

$$d_j^n = \frac{\varphi^\flat(u) - u}{\varphi^\flat(u) - \varphi^{-\flat}(u)}.$$

The property $0 \leq d_j^n \leq 1$ means $\min(\varphi^{-\flat}(u), \varphi^\flat(u)) \leq u \leq \max(\varphi^{-\flat}(u), \varphi^\flat(u))$ and cannot hold, since u and $\varphi^\flat(u)$ do not have the same sign for all u. Then, we obtain $f_{j+1/2}^n = f(u)$ if $f' \geq 0$ and $f_{j-1/2}^n = f(u)$ if $f' \leq 0$ by (21)-(23).

Proof of Property 2. Assume without restriction that $f' \geq 0$ and recall that $0 \leq d_{j-1}^n \leq 1$ and $0 \leq d_j^n \leq 1$ respectively means that $\min(\varphi^{-\flat}(u_j^n), \varphi^\flat(u_{j-2}^n)) \leq u_{j-1}^n \leq \max(\varphi^{-\flat}(u_j^n), \varphi^\flat(u_{j-2}^n))$ and $\min(\varphi^{-\flat}(u_{j+1}^n), \varphi^\flat(u_{j-1}^n)) \leq u_j^n \leq \max(\varphi^{-\flat}(u_{j+1}^n), \varphi^\flat(u_{j-1}^n))$. These inequalities are not valid since by definition u and $\varphi^\flat(u)$ do not belong to the same region of convexity of f. By (21)-(23), the numerical fluxes $f_{j\pm1/2}^n$ coincides with the usual upwind fluxes and the conclusion follows.

Proof of Property 3. First, note that there is no relevant reconstruction in the first iteration. Indeed, the property $0 \leq d_j^n \leq 1$ reads as follows if $j < 0$ or $j > 1$,

$$0 \leq d_j^n \leq 1 \text{ if and only if } \begin{cases} \min(\varphi^{-\flat}(u_l), \varphi^\flat(u_l)) \leq u_l \leq \max(\varphi^{-\flat}(u_l), \varphi^\flat(u_l)), & j < 0, \\ \min(\varphi^{-\flat}(u_r), \varphi^\flat(u_r)) \leq u_r \leq \max(\varphi^{-\flat}(u_r), \varphi^\flat(u_r)), & j > 1, \end{cases}$$

which again cannot hold (see (i) below), while if $j = 0$ or $j = 1$, the relation $u_r = \varphi^\flat(u_l)$ and definition (14) give

$$\begin{cases} d_j^n = \dfrac{u_r - u_l}{u_r - u_l} = 1, & j = 0, \\ d_j^n = \dfrac{u_r - u_r}{u_r - u_l} = 0, & j = 1, \end{cases}$$

so that the reconstructions exist but are trivial: $u_l = \varphi^{-\flat}(u_r)$ (respectively $u_r = \varphi^\flat(u_l)$) takes the whole cell associated with $j = 0$ (respectively $j = 1$).
Assume now without restriction that f is non-decreasing and let Δt be such that (25) holds. After one time step Δt, the exact solution given by $u(x, \Delta t) = u_l$ if $x < \sigma(u_l, u_r)\Delta t$ and $u(x, \Delta t) = u_r$ otherwise is such that

$$\frac{1}{\Delta x}\int_{x_{j-1/2}}^{x_{j+1/2}} u(x, \Delta t)dx = \begin{cases} u_l, & j \le 0, \\ u_r - \sigma(u_l, u_r)\frac{\Delta t}{\Delta x}(u_r - u_l), & j = 1, \\ u_r, & j > 1. \end{cases} \tag{27}$$

But recall that $\sigma(u_l, u_r)$ is given by (17) so that we have

$$\frac{1}{\Delta x}\int_{x_{j-1/2}}^{x_{j+1/2}} u(x, \Delta t)dx = \begin{cases} u_l - \frac{\Delta t}{\Delta x}(f(u_l) - f(u_l)), & j \le 0, \\ u_r - \frac{\Delta t}{\Delta x}(f(u_r) - f(u_l)), & j = 1, \\ u_r - \frac{\Delta t}{\Delta x}(f(u_r) - f(u_r)), & j > 1, \end{cases} \tag{28}$$

that is

$$u_j^1 = \frac{1}{\Delta x}\int_{x_{j-1/2}}^{x_{j+1/2}} u(x, \Delta t)dx, \qquad j \in \mathbb{Z}. \tag{29}$$

The identity (26) is then proved for the first iterate.
What happens now in the next time iteration ? At this stage, it is first clear (see the previous discussion just below) that only cell $\mathcal{C}_1$ is going to be dealt with a reconstruction. Now, the main point of the proof lies in the fact that the reconstructed discontinuity in this cell actually joins the expected states $\varphi^{-\flat}(u_2^1) = \varphi^{-\flat}(u_r) = u_l$ and $\varphi^\flat(u_0^1) = \varphi^\flat(u_l) = u_r$ and is located exactly at point $x = \sigma(u_l, u_r)\Delta t$ by the conservation property (29). In other words, we have reconstructed the exact solution at time $t = \Delta t$. To derive the required identity (26) for the second iterate, it is sufficient to recall that by Green's formula the conservative scheme (11) with $f_{j+1/2}^n$ defined for all $j \in \mathbb{Z}$ by (21)-(23) is equivalent for $n = 2$ to average the evolution of this exact solution up to time $t^2 = 2\Delta t$. And the process is going on in a similar way for the next time iterations, which proves the result.

5 Numerical experiments

We mostly consider here the flux $f(u) := u^3 + u$, thus f is concave-convex in the sense given in the second section. For the entropy-entropy flux pair (U, F) required in (2), we use

$$U(u) := u^2, \quad F(u) := \frac{3}{2}u^4 + u^2.$$

Easy calculations lead to explicit formulas for $\varphi^\natural$ and $\varphi^{-\natural}$:

$$\varphi^\natural = -\frac{u}{2}, \qquad \varphi^{-\natural} = -2u, \qquad \varphi_0^\flat(u) = -u.$$

Moreover, we have here $\varphi^\sharp(u) = -u - \varphi^\flat(u)$.

The choice of the kinetic function $\varphi^\flat$ must be in agreement with relations (8) with $\varphi^\sharp$ and $\varphi_0^\flat$ just calculated. Here, we will choose the kinetic function

$$\varphi^\flat(u) = -\beta u, \quad \beta \in [0.5, 1)\,,$$

which, as observed in Bedjaoui and LeFloch [3], can be realized by an augmented model based on nonlinear diffusion and dispersion terms. In the following, we will take $\beta = 0.75$.

Test A. Let us check Property 3 numerically, which is concerned with the exact capture of isolated nonclassical shocks. Thus, consider the following nonclassical shock as a Riemann initial condition

$$u_0(x) = \begin{cases} 4, & x < 0, \\ \varphi^\flat(4) = -3, & x > 0, \end{cases}$$

The numerical solution shown in Figure 5 is exact everywhere but in the single cell containing the nonclassical shock. (We sometimes use a piecewise constant representation in the figure, in order for the interpretation of the numerical solutions to be easier.) However, as expected, the value in this cell coincides with the average of the corresponding exact solution (see (26)), and allows (after reconstruction) to recover the *exact* location of the discontinuity (using the conservation property of scheme). This property explains why the numerical solution stays sharp when the time evolves.

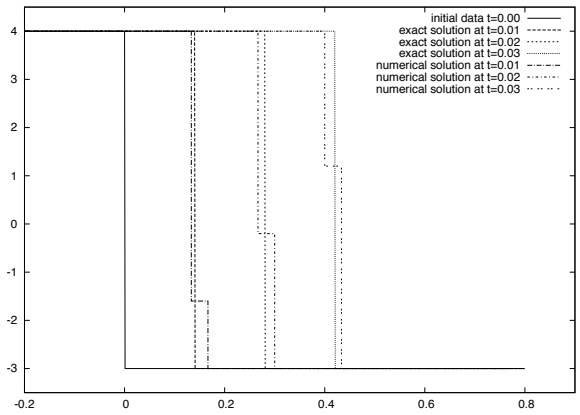

Figure 5: Test A - Nonclassical shock – 30 points

Test B. In our second test we consider the Riemann problem with initial data

$$u_0(x) = \begin{cases} 4, & x < 0, \\ -5, & x > 0, \end{cases}$$

whose solution is a nonclassical shock followed by a rarefaction wave. The two left-hand curves in Figure 6 are performed with $\Delta x = 0.01$ and $\Delta x = 0.002$, respectively. The nonclassical shock, as previously, is localized in a single computational cell.
The right-hand figure represents the logarithm of the L^1-error (between the exact and the numerical solution) versus the logarithm of Δx. The numerical order of convergence is about 0.8374.

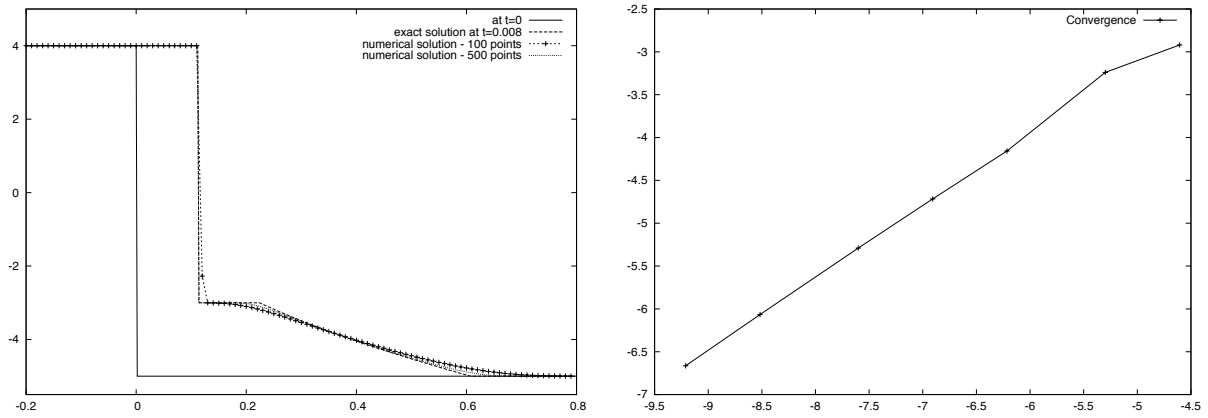

Figure 6: Test B - Nonclassical shock and rarefaction – L^1 convergence ($\log(E_{L^1})$ versus $\log(\Delta x)$)

Test C (Figure 7). Now, we choose another Riemann initial condition which develops a nonclassical shock followed by a classical shock:

$$u_0(x) = \begin{cases} 4, & x < 0, \\ -2, & x > 0. \end{cases}$$

We can make the same observation as previously, concerning the nonclassical shock; it is sharply captured and arises in a small spatial domain. However, note here that the classical shock does contain some numerical diffusion: in fact, our scheme is exactly the upwinding scheme if the values of the solution remains in a given convexity region for the flux f.
Once again, the plot with the L^1-error shows the numerical convergence with order about 0.9999.

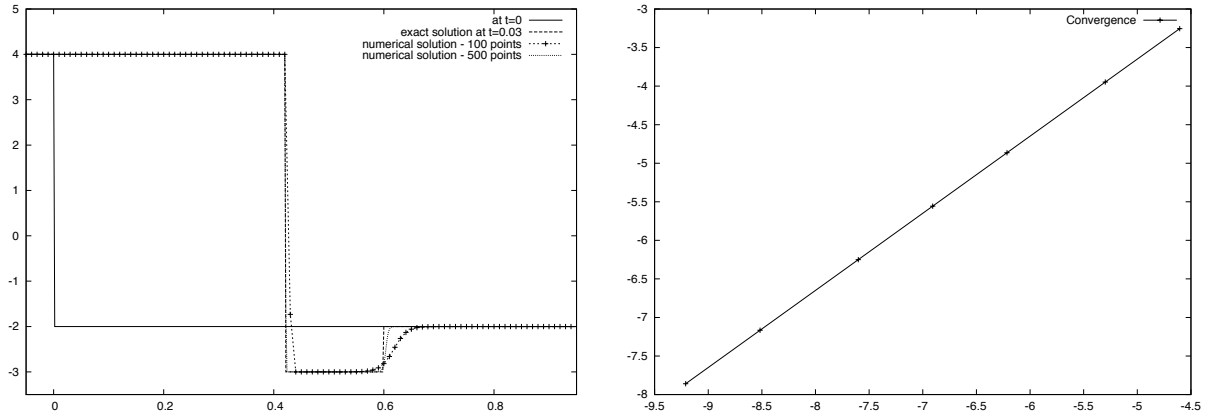

Figure 7: Test C - Nonclassical and classical shocks – L^1 convergence ($\log(E_{L^1})$ versus $\log(\Delta x)$)

Test D (Figure 8). We now take an initial data composed of two nonclassical shocks that interact:

$$u_0(x) = \begin{cases} 4 = \varphi^{-\flat}(-3), & x < 0.1 \\ -3, & 0.1 < x < 0.2 \\ 2.25 = \varphi^{\flat}(-3), & x > 0.2. \end{cases}$$

The computation is performed with $\Delta x = 0.05$ and plotted at four successive times $t = 0, 0.0010, 0.0017,$ and 0.0020. We observe that the two nonclassical shocks cancel each other at the interaction, and generate a single classical shock, in accordance with the general theory in [21].

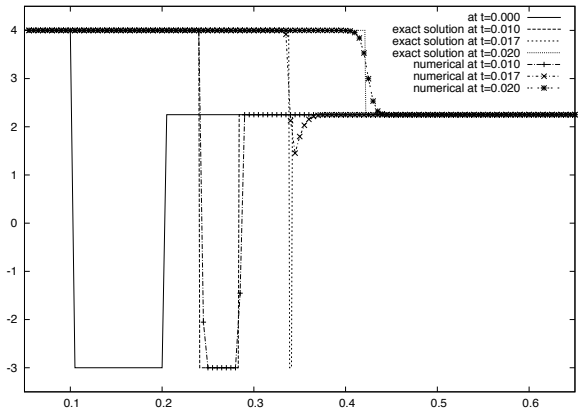

Figure 8: Test D - Interaction of two nonclassical shocks

Test E (Figure 9). Next, we consider the periodic initial condition

$$u_0(x) = \sin\left(\frac{x}{2\pi}\right),$$

with periodic boundary conditions $u(-0.5, t) = u(0.5, t)$. The exact solution is not known explicitly, so we compare our numerical solution with the solution generated by Glimm's random choice scheme [12] in which we have replaced the classical solver by the nonclassical solver described in Section 2. We use here van der Corput's random sequence (a_n), defined by

$$a_n = \sum_{k=0}^{m} i_k 2^{-(k+1)},$$

where $n = \sum_{k=0}^{m} i_k 2^k$, $i_k \in \{0, 1\}$, denotes the binary expansion of the integer n. Figure 9 represents the solutions at the times $t = 0, 0.25$ and 0.5 for our scheme with $\Delta x = 0.01$ and with $\Delta x = 0.0001$, and for the Glimm scheme with $\Delta x = 0.0001$ (to serve as a reference). The two methods strongly agree. Roughly speaking, the increasing parts of u_0 evolve as rarefactions, while the decreasing parts are compressed and develop in a classical shock and, then, when left- and right-hand states at the shocks change sign, nonclassical shocks (which do satisfy the expected kinetic relation) and new faster classical shocks on the right-hand side arise.

Test F (Figure 10). To illustrate the behavior of convex-concave flux functions, we finally compute two Riemann solutions with opposite flux $f(u) = -u^3 - u$ (so $f' < 0$ and the solutions move from right to left) and the same kinetic function $\varphi^\flat(u) = -0.75\ u$: the first one (left-hand figure) corresponds to the initial data

$$u_0(x) = \begin{cases} -4, & x < 0, \\ 4, & x > 0, \end{cases}$$

and develops a rarefaction wave and a nonclassical shock; the second one (right-hand figure) corresponds to the initial data

$$u_0(x) = \begin{cases} -2, & x < 0, \\ 4, & x > 0, \end{cases}$$

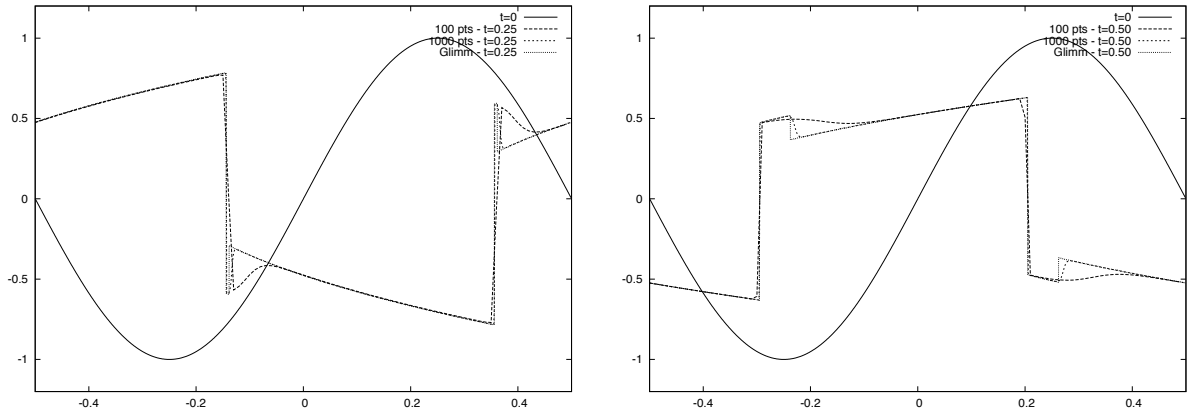

Figure 9: Test E - Periodic initial data - reconstruction scheme and Glimm scheme

and the corresponding solution is a classical shock followed by a nonclassical shock.

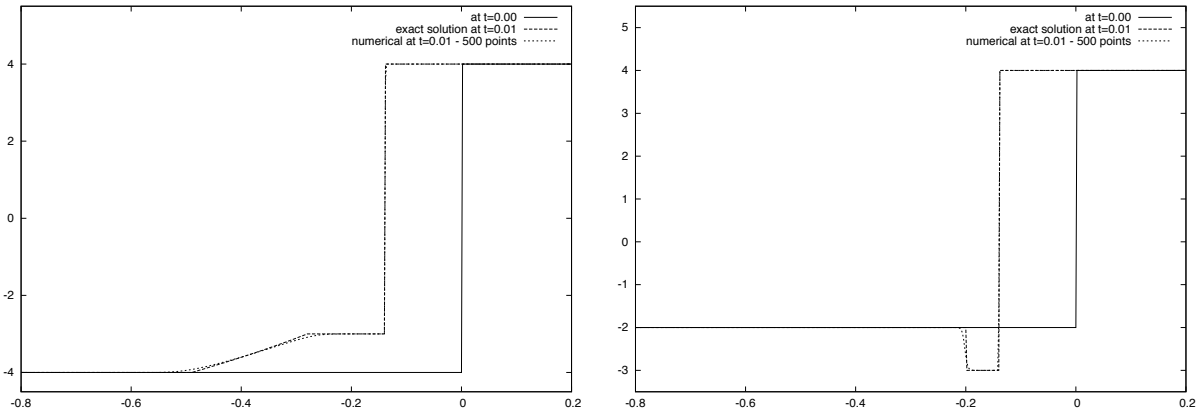

Figure 10: Test E - Two examples in the convex-concave case

Test F. We now study how the kinetic relation $u_R = \varphi^\flat(u_L)$ is computed. On Figure 11 (right-hand figure), we plot points whose horizontal coordinates (respectively vertical coordinates) correspond to the left-hand (resp. right-hand) traces around the reconstructed cell. The initial data allows us to cover a large range of value:

$$u_0(x) = \begin{cases} 0, & x < 0.5, \\ 1 + 20(x + 0.45), & 0.5 < x < 0.45, \\ -0.75, & x > -0.45. \end{cases}$$

The left-hand figure represents the solution at different times with $\Delta x = 0.0002$.

We clearly observe the convergence of the numerical kinetic relation towards the prescribed one. This a strong test to validate the proposed method.

Test G. In the course of designing the scheme proposed in the previous section we tried several variants. We report here one such scheme that is very similar to the proposed scheme,

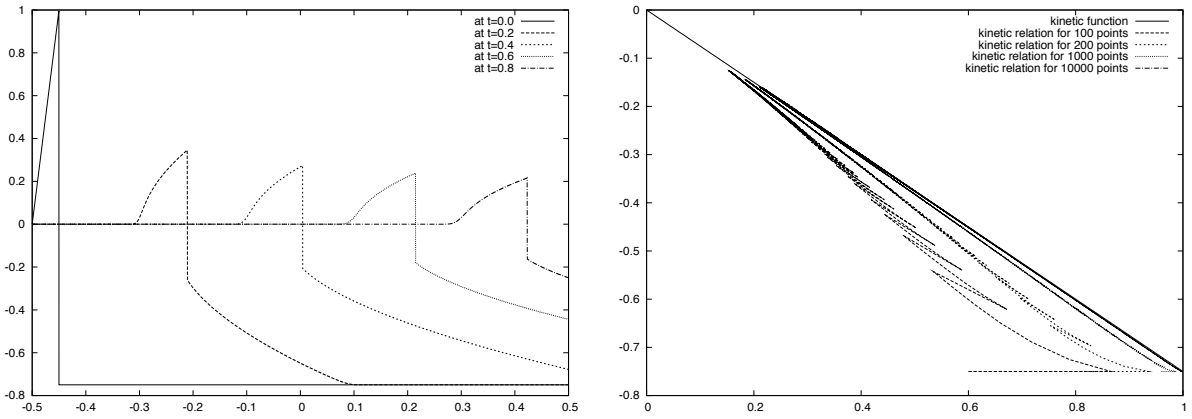

Figure 11: Test F - Numerical kinetic relation

but which *does not* converge to exact nonclassical solutions. This is due to the fact that small oscillations are generated in the scheme which are in competition with the dissipation mechanisms described by the prescribed kinetic function.

The variant is designed for the concave-convex flux $f(u) = u^3 + u$. The only difference with the scheme developed above is that it performs the reconstruction in $\mathcal{C}_j$ with $u^n_{j,l} = u^n_{j-1}$ (instead of $\varphi^{-\flat}(u^n_{j+1})$ and $u_{j,r} = \varphi^{\flat}(u^n_{j-1})$. This is equivalent in the case of a *pure* nonclassical shock (Test B) but different in the general case.
Figure 12 presents the solution obtained for the same initial value as in Test E. Oscillations are generated because the reconstruction is not constrained enough in this version of the scheme.

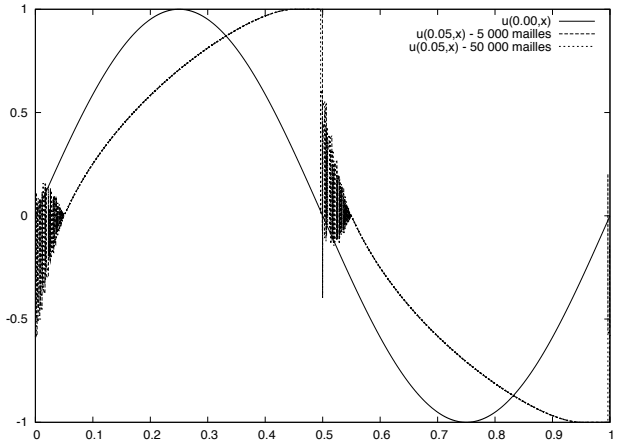

Figure 12: Another version of the scheme

6 Concluding remarks

In this paper we have introduced a new numerical strategy for computing nonclassical solutions to nonlinear hyperbolic conservation laws. The method is based on a reconstruction technique

performed in each computational cell which may exhibit a nonclassical shock. Importantly, the whole algorithm is *conservative* and propagates any admissible nonclassical discontinuity exactly. The convergence of the proposed method was demonstrated numerically for several test-cases. This new approach brings a new perspective on the numerical approximation of nonclassical shocks and kinetic functions. The efficiency of the method is clearly demonstrated in the present paper, and we refer to the follow-up paper [4] for various extensions and applications. Among the questions of interest we can mention the total variation bounds and the hyperbolic systems of conservation laws, the application to real materials undergoing phase transitions, as well as the extension to higher-order schemes.

References

[1] Abeyaratne R. and Knowles J.K., Kinetic relations and the propagation of phase boundaries in solids, Arch. Ration. Mech. Anal., vol 114, pp 119–154 (1991).

[2] Abeyaratne R. and Knowles J.K., *Implications of viscosity and strain gradient effects for the kinetics of propagating phase boundaries*, SIAM J. Appl. Math., vol 51, pp 1205–1221 (1991).

[3] Bedjaoui N. and LeFloch P.G., Diffusive-dispersive traveling waves and kinetic relations V. Singular diffusion and nonlinear dispersion, Proc. Royal Soc. Edinburgh, vol 134A, pp 815–843 (2004).

[4] Boutin B., Chalons C., Lagoutière F., and LeFloch P.G., *Convergent and conservative schemes for nonclassical solutions based on kinetic relations. II*, in preparation.

[5] Chalons C., *Transport-equilibrium schemes for computing nonclassical shocks. Scalar conservation laws*, preprint available at http://www.math.ntnu.no/conservation/2006/051.html.

[6] Chalons C., *Numerical approximation of a macroscopic model of pedestrian flows*, SIAM J. Sci. Comput. (2007), to appear.

[7] Chalons C. and LeFloch P.G., *A fully discrete scheme for diffusive-dispersive conservation laws*, Nümerische Math., vol 89, pp 493–509 (2001).

[8] Chalons C. and LeFloch P.G., *High-order entropy conservative schemes and kinetic relations for van der Waals fluids*, J. Comput. Phys., vol 167, pp 1-23 (2001).

[9] Chalons C. and LeFloch P.G., *Computing undercompressive waves with the random choice scheme. Nonclassical shock waves*, Interfaces and Free Boundaries, vol 5, pp 129–158 (2003).

[10] Després B. and Lagoutière F., *Contact discontinuity capturing schemes for linear advection and compressible gas dynamics*, SIAM J. Sci. Comput., vol 16, pp 479–524 (2001).

[11] Fan H.-T. and Slemrod M., The Riemann problem for systems of conservation laws of mixed type, in "Shock induced transitions and phase structures in general media", Workshop held in Minneapolis (USA), Oct. 1990, Dunn J.E. (ed.) et al., IMA Vol. Math. Appl. 52 (1993), pp. 61-91.

[12] Glimm J., *Solutions in the large time for nonlinear hyperbolic systems of equations*, Comm. Pure Appl. Math., vol 18, pp 697-715 (1965).

[13] Hayes B.T. and LeFloch P.G., Nonclassical shocks and kinetic relations: Scalar conservation laws, Arch. Ration. Mech. Anal., vol 139, pp 1–56 (1997).

[14] Hayes B.T. and LeFloch P.G., *Nonclassical shocks and kinetic relations : Finite difference schemes*, SIAM J. Numer. Anal., vol 35, pp 2169–2194 (1998).

[15] Hou T.Y., LeFloch P.G., and Rosakis P., *A level-set approach to the computation of twinning and phase transition dynamics*, J. Comput. Phys., vol 150, pp 302–331 (1999).

[16] Hou T.Y., LeFloch P.G., and Zhong X., *Converging methods for the computation of propagating solid-solid phase boundaries*, J. Comput. Phys., vol 124, pp 192–216 (1996).

[17] Lagoutière F., *Modélisation mathématique et résolution numérique de problèmes de fluides compressibles à plusieurs constituants*, Thèse de l'Université Paris VI, (2000).

[18] Lagoutière F., *Stability of reconstruction schemes for scalar hyperbolic conservation laws*, submitted (2007).

[19] Lagoutière F., *Non-dissipative entropic discontinuous reconstruction schemes for hyperbolic conservation laws*, submitted (2007).

[20] LeFloch P.G., *Propagating phase boundaries: formulation of the problem and existence via the Glimm scheme*, Arch. Rational Mech. Anal., vol 123, pp 153–197 (1993).

[21] LeFloch P.G., *Hyperbolic Systems of Conservation Laws: The theory of classical and nonclassical shock waves*, E.T.H. Lecture Notes Series, Birkhäuser, 2002.

[22] LeFloch P.G. and Rohde C., *High-order schemes, entropy inequalities, and nonclassical shocks*, SIAM J. Numer. Anal., vol 37, pp 2023–2060 (2000).

[23] LeFloch P.G. and Shearer M., *Nonclassical Riemann solvers with nucleation*, Proc. Royal Soc. Edinburgh, vol 134A, pp 941–964 (2004).

[24] Merkle C. and Rohde C., *Computations of dynamical phase transitions in solids*, Appl. Numer. Math. Vol. 56 (10/11), pp 1450–1463 (2006).

[25] Merkle C. and Rohde C., *The sharp-interface approach for fluids with phase change: Riemann problems and ghost fluid techniques*, Preprint-Reihe IANS, Universität Stuttgart (2006).

[26] Schulze S. and Shearer M., Undercompressive shocks for a system of hyperbolic conservation laws with cubic nonlinearity, J. Math. Anal. Appl. vol 229, pp 344–362 (1999).

[27] Shearer M. and Yang Y., The Riemann problem for the p-system of conservation laws of mixed type with a cubic nonlinearity, Proc. A Royal Soc. Edinburgh., vol 125A, pp 675–699 (1995).

[28] Slemrod M., Admissibility criteria for propagating phase boundaries in a van der Waals fluid, Arch. Ration. Mech. Anal., vol 81, pp 301–315 (1983).

[29] Slemrod M., A limiting viscosity approach to the Riemann problem for materials exhibiting change of phase, Arch. Ration. Mech. Anal., vol 105, pp 327–365 (1989).

[30] Truskinovsky L., Dynamics of non-equilibrium phase boundaries in a heat conducting nonlinear elastic medium, J. Appl. Math. and Mech., vol 51, pp 777–784 (1987).

[31] Truskinovsky L., Kinks versus shocks, in "Shock induced transitions and phase structures in general media", R. Fosdick, E. Dunn, and M. Slemrod ed., IMA Vol. Math. Appl., Vol. 52, Springer-Verlag, New York (1993), pp. 185–229.